



## Statistical estimates of rock-free lunar regolith thickness from diviner

Jaahnavee Venkatraman<sup>\*</sup>, Tyler Horvath, Tyler M. Powell, David A. Paige

Department of Earth, Planetary, and Space Sciences, University of California, Los Angeles, 595 Charles E Young Dr E, 90095, USA



### ARTICLE INFO

#### Keywords:

Moon  
Regolith  
Rock abundance  
LRO Diviner  
Crater statistics

### ABSTRACT

The thickness of the lunar regolith has been previously estimated using seismic, radar, and crater morphology data to be on the order of 10 m. In this study, we use rock abundance measurements from the Diviner radiometer aboard the Lunar Reconnaissance Orbiter (LRO) to provide new estimates of rock-free regolith thickness in recently-formed impact craters. Diviner cold spots have been shown to last no longer than a few 100 kyr, and thereby point to fresh craters on the Moon. Trends in Diviner data also show that larger, and therefore deeper, cold spot craters have rockier ejecta. We employ statistical analyses to show that cold spot craters in the lunar mare have rockier ejecta at smaller excavation depths when compared to those in the highlands. We estimate that the average rock-free regolith is approximately 10 m thick in the mare and 12 m thick in the highlands, which is consistent with previous estimates. We expect these values will be highly variable due to differences in regolith development and overturn across the Moon.

### 1. Introduction

The lunar regolith covers the entire surface of the Moon and is in direct contact with the surrounding space environment. As an airless body, the Moon preserves geologic evidence on its surface (McKay et al., 1991). Naturally it follows that the lunar regolith is our primary source of geological and geophysical information about the Moon (Fa and Wieczorek, 2012; Hayne et al., 2017; Hörz et al., 1991; Shkuratov and Bondarenko, 2001; National Aeronautics and Space Administration, 1994). Recent evidence also suggests that the lunar regolith may harbor valuable resources, including volatile ices, near the lunar poles (Colaprete et al., 2010; Fisher et al., 2017; Hayne et al., 2015; Li et al., 2018; Rubanenko et al., 2019). Understanding how thick the lunar regolith is i.e. to what depth below the Moon's surface the soil is fine-grained and rock-free, is key to advancing these scientific efforts, particularly in light of the Artemis program and its science objectives (National Aeronautics and Space Administration, 2020).

The presence of boulder fields on the Moon's surface and buried beneath the regolith fines have historically been an obstacle for lunar landings. During the Apollo 11 descent, the crew was forced to perform a spontaneous, semi-manual maneuver to avoid blocky ejecta approximately 400 m east of the ultimate landing site with only 25 s of fuel remaining (Apollo 11 mission report, 1969). For Apollo 12, the actual landing point was determined in real time from visible surface features (Apollo 12 mission report, 1970). Although confirmed with other

measurements from lunar orbit, none of these methods were individually precise enough to establish the landing site within a few feet of known features (Apollo 12 mission report, 1970). Rock abundance (RA) measurements from the Lunar Reconnaissance Orbiter (LRO) Diviner Lunar Radiometer Experiment provide a means to begin quantifying the distribution of these boulders on the surface. Diviner-derived RA is the fraction of surface area covered by boulders in a single Diviner pixel (Bandfield et al., 2011). Combined with data from fresh impacts, this can inform us about the distribution of subsurface consolidated rock using regolith thickness estimates.

#### 1.1. Previous work

There have been extensive prior efforts to characterize the approximate thickness of the lunar regolith. Results from Apollo seismic data (Hörz et al., 1991) divide the upper 25 km of the lunar surface into approximately a 10 m thick regolith, followed by large scale ejecta up to the 2 km mark, and crust up to roughly 25 km (Fig. 1). Quaide and Oberbeck (1968), and later Bart et al. (2011), attempted to find regolith thickness distributions using crater morphology. Their results showed thicknesses on the order of 10 m, which concurs with previous studies. However, Prieur et al. (2018) have shown that crater morphology does not necessarily follow a typical trend with diameter. The global distribution of regolith thickness on the Moon has also been studied extensively using radar data. Work by Shkuratov and Bondarenko (2001) and

<sup>\*</sup> Corresponding author.

E-mail address: [jaahnavee96@ucla.edu](mailto:jaahnavee96@ucla.edu) (J. Venkatraman).

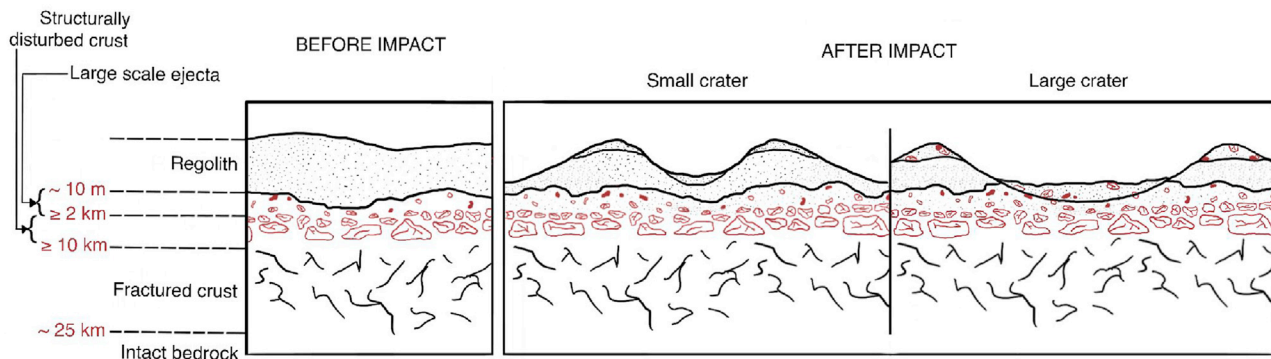


Fig. 1. Schematic of penetration depths and corresponding ejecta for a small crater and large crater, assuming the uppermost lunar surface layers from Hörz et al. (1991).

Fa and Wieczorek (2012) use 70 cm Aricebo data and find regolith thicknesses ranging from 2 to 17 m. However, this approach cannot be applied to regions where the surface roughness is very high as radar sounder echoes are affected by surface clutter from rocky, off-nadir impact craters (Fa and Wieczorek, 2012). Wilcox et al. (2005) inferred regolith depths in an equivalent range, but using crater size frequency distribution statistics. Similar to Shoemaker and Morris (1970), they define regolith thickness using the distribution of missing craters obliterated by repetitive impact processes. They observed that the depth of the regolith is equal to the excavation depth of the largest saturated craters. It is important to note that all of these estimates fall within ranges. Both Shkuratov and Bondarenko (2001) and Fa and Wieczorek (2012) find that the mare regolith is a few meters thinner than that in the highlands. We expect our estimates in this study to vary by lunar region as well due to differences in impact gardening, and the resulting differences in regolith overturn across the Moon (Quaide and Oberbeck, 1968).

### 1.2. Lunar regolith geology

There is disagreement in the literature as to what constitutes the lunar regolith. Arnold (1975) notes this ambiguity in his Monte Carlo model for lunar regolith gardening. The Lunar Sourcebook uses the terms soil and regolith interchangeably, defining them as fragmental, unconsolidated rock material - residual or transported - at the lunar surface (Hörz et al., 1991). Others have defined it in terms of process of formation. Shoemaker and Morris (1970) describe the regolith to be low cohesion material formed by repetitive bombardment, covering nearly all parts of the lunar surface. Their definition distinguishes this heavily reworked layer from the larger debris or rocks underlying this layer. There is some doubt as to whether such a 'megaregolith' layer might exist, and what it constitutes. Oberbeck et al. (1973) discuss how the regolith itself is not completely reworked, rather interspersed with coarser-grained material, creating an ambiguous boundary between the regolith and so-called megaregolith. We do not attempt to define the megaregolith in the present work. We are primarily concerned with rock detectable by Diviner and regolith that is rock-free.

We also know that there are differences between the geology of the mare and highlands regolith. It has been shown that there is a well-defined deposit of basalts under the mare regolith that stems from past lunar volcanism (Wilhelms and with, 1987). Using radar data, Fa et al. (2015) have also shown the presence of a relatively homogenous 'Paleoregolith' in the mare region around the Chang'e 3 landing site that could be buried beneath crater ejecta. The lunar highlands, which have been pulverized from accumulated impacts, are geologically more complex than the mare (Cintala and Mcbride, 1995). The exact structure and composition of the highlands subsurface is still under debate. Seismic measurements do not show a pronounced discontinuity between the regolith-bedrock interface in the highlands. This could point to the

presence of highland impact breccia from sufficiently heated ejecta that cemented beneath the regolith but above larger rock (Hörz et al., 1991).

### 1.3. Diviner rock abundance and cold spots

In the present work, we calculate rock-free regolith thickness statistically, using the LRO Diviner Lunar Radiometer (Paige et al., 2010) RA estimates from cold spot craters, which are visibly fresh impact craters surrounded by a large region of reduced nighttime temperatures (Bandfield et al., 2014).

Since consolidated rock has a higher thermal inertia than fine-grained regolith, surface temperatures derived from Diviner measurements provide a means to understand physical properties such as RA on the lunar surface (Bandfield et al., 2011). Using this method, Diviner is able to detect rocks larger than 1 m in diameter. Fig. 1 illustrates the potential utility of surface RA measurements for probing subsurface material. Larger craters will naturally excavate deeper into the lunar surface. It is expected that small impact craters will excavate only regolith, while larger craters will excavate more consolidated rock detectable by Diviner (Fig. 1). We therefore expect to be able to measure lunar regolith thickness as the depth at which these craters excavate consolidated rock detectable by Diviner.

RA signatures have, however, been shown to fade over time (Ghent et al., 2014). Basilevsky et al. (2013) have also shown that the median survival time of meter-sized boulders on the rims of smaller craters on the Moon's surface is between just 40 and 80 Ma. Thus, focusing on fresh, young craters is of particular importance. Cold spots on the Moon provide us with the ability to constrain our database of craters to ones that are fresh and young. Williams et al. (2018) have shown that smaller cold spots around lunar craters persist for ~100 ka to 1 Ma, and therefore point to fresh, young impact craters with an enduring RA signature. Using the LRO Diviner Lunar Radiometer RA estimates from cold spot craters, we can statistically estimate rock-free regolith thickness.

## 2. Methods

Our approach to find regolith thickness estimates involves statistically quantifying the depth at which small, simple, and fresh craters begin to excavate rock detectable by Diviner. To do so, we compare the diameters and calculated excavation depths for each crater in our dataset against Normalized RA (NRA) calculated as  $RA_{max} - RA_{mean}$  (see section 2.1), to find the average depth at which small, simple, cold spot craters exceed a certain threshold NRA value, indicating that they have excavated consolidated rock beneath the fine-grained regolith. We expect to see a difference between the lunar mare and highlands excavation depth values, similar to previous estimates (Fa and Wieczorek, 2012; Hörz et al., 1991; Shkuratov and Bondarenko, 2001; Quaide and Oberbeck, 1968; Bart et al., 2011; Wilcox et al., 2005; Shoemaker and Morris,

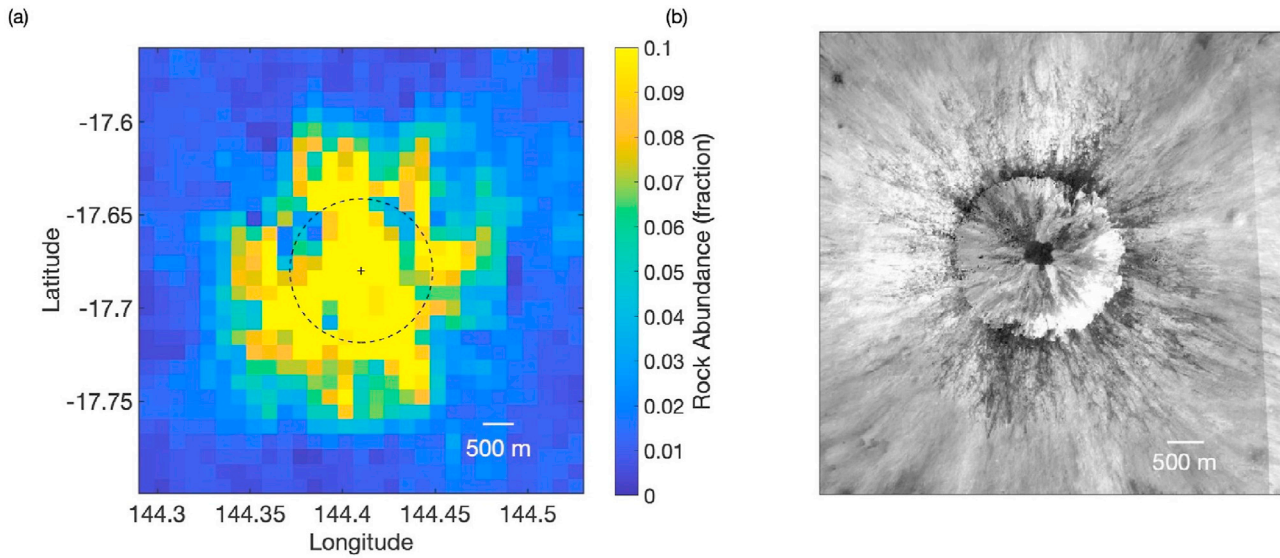


**Fig. 2.** (a) Example of Diviner derived RA for a 2.3 km diameter cold spot crater located at 4.079°S, 151.682°E. The black dashed line represents the rim of the crater centered at '+'. (b) LROC NAC (Robinson et al., 2010; Robinson, 2010; Humm et al., 2016; Mahanti et al., 2016) Mosaic of images M125984243RE, M1222726789RE, and M1222726789LE corresponding to subfigure (a). Both images have a horizontal and vertical extend of three crater radii.

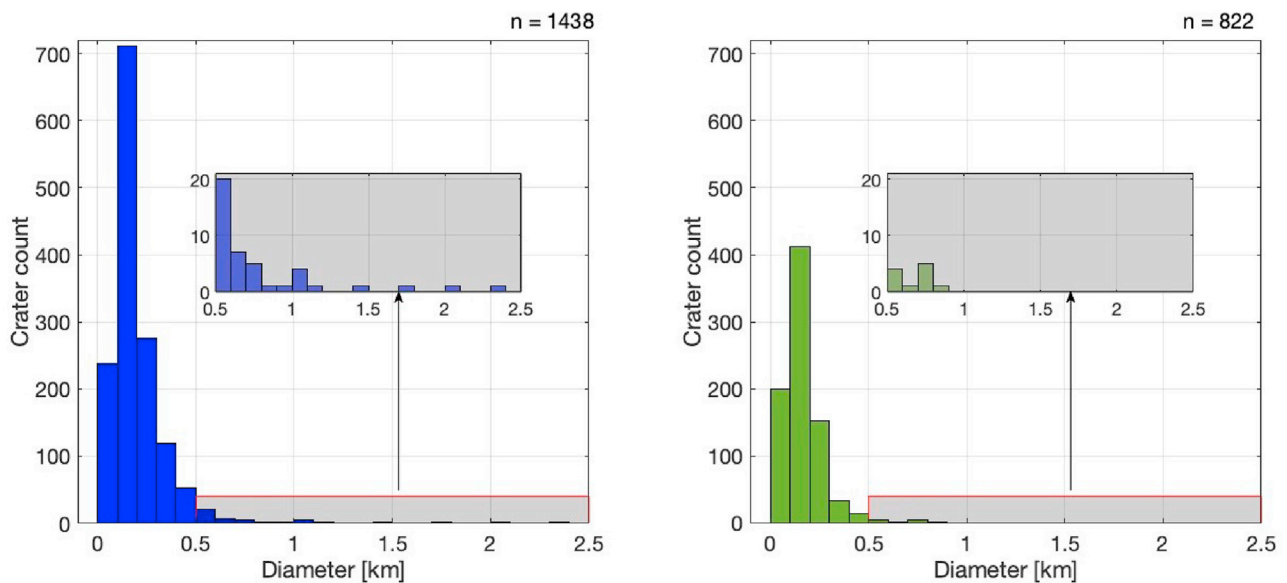


**Fig. 3.** Distribution of diameters for all cold spot craters in our RA dataset, for the highlands (left) and mare (right). Bin width of the histograms is 0.1 km. The inset plots show the tail-end of the distributions to highlight that simple cold spot craters at larger diameters occur less frequently in our dataset.

1970).

### 2.1. Normalized rock abundance

For the present study we used an updated version (Venkatraman et al., 2022) of the Williams et al. (2018) cold spot dataset to find the centers and diameters of 2282 cold spot craters, ranging from 43 m to 2.3 km in diameter, equatorward of  $\pm 50^\circ$  latitude. We identified the center of each cold spot crater in both LROC NAC images and the Diviner 128 pixels per degree (240 m per pixel at the equator) improved global RA maps (Bandfield et al., 2011; Williams et al., 2017; Powell et al., 2022), as illustrated in Fig. 2. Most debris ejected by an impact crater falls within one crater diameter from the rim (Melosh, 1989). We therefore calculated the value of maximum and mean RA for the crater interior and surrounding ejecta within three radii from the center of that crater

(Fig. 2). We use normalized Diviner RA (NRA) to distinguish ejecta rock values from the background regolith (all regolith away from the ejecta). While background regolith RA values are normally distributed, ejecta values are not (Ghent et al., 2014). Ejecta RA distributions are typically right-skewed and cannot be meaningfully represented by Gaussian summary statistics like the mean RA (Ghent et al., 2014). To effectively capture the right skew of the RA distribution for each crater, we calculate NRA as  $RA_{max} - RA_{mean}$  of the region within three radii of the crater center. This is simply a heuristic method of capturing the skewness of a distribution by incorporating the distribution maxima. This statistic can be refined in future studies with the availability of more data (Behrens et al., 2004; Sohn et al., 2005). Our derived NRA dataset contains 22 craters less than the Williams et al. (2018) cold spot dataset as a result of missing information in the global RA maps. Our crater diameters for this study are right-skewed, following a power law distribution, with

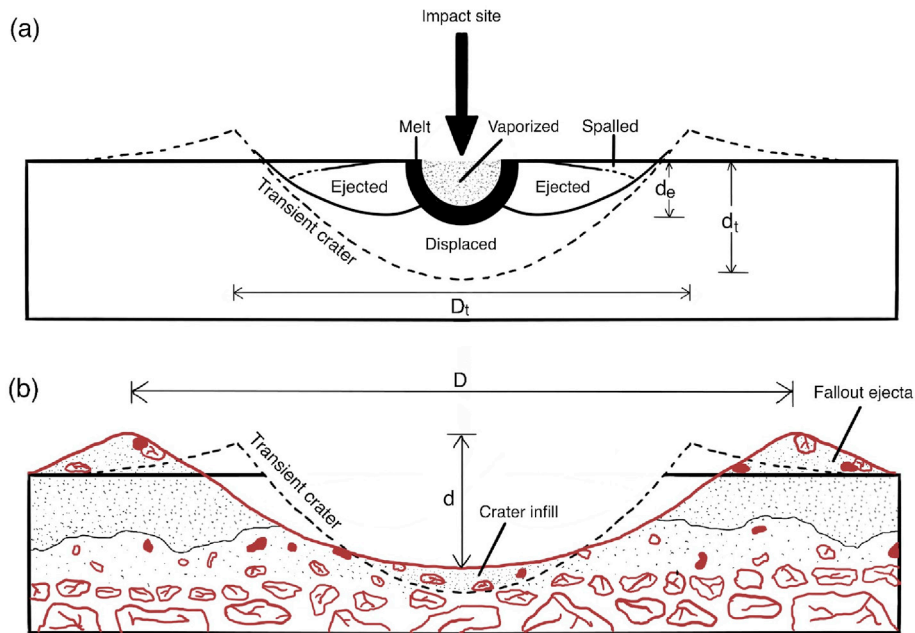


**Fig. 4.** (a) Shows a schematic of crater modification and movement of material during the formation of a typical small, simple crater (from Melosh (1989), Fig. 6.8, p. 238). (b) Shows the difference between the dimensions and nature of excavated material of transient and final crater boundaries post gravity-dominated collapse. Adapted from Grieve (1987).

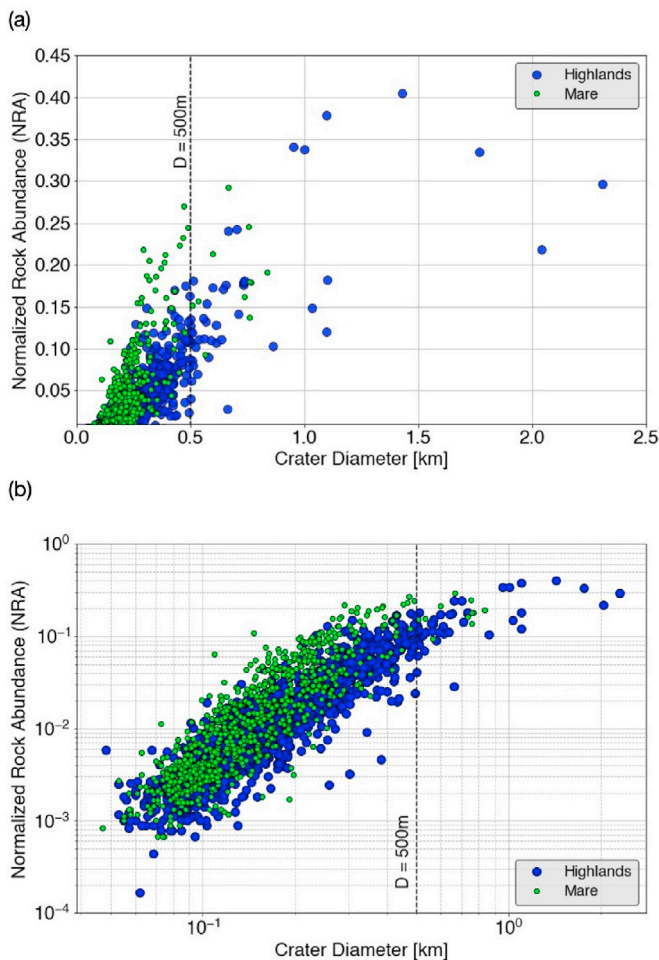


**Fig. 5.** (a) Linear and (b) log-log scatterplots of cold spot crater diameter against NRA for the lunar mare and highlands.

approximately 97% having diameters less than 500 m (Fig. 3).

### 2.2. Excavation depth

There are numerous processes that tend to affect the depth of small, strength-dominated craters, including ejection of crater material, displacement of material out of the crater deforming adjacent rocks, and the formation of a brief transient crater (Fig. 4a). The apparent depths ( $d$ ) of these young, small, strength-dominated craters are 0.2 times their diameters ( $D$ ) (Fig. 4b) which can be written as:

$$d = 0.2 D \quad [42] \tag{1}$$

Below a diameter of approximately 130 m however, the  $d/D$  ratio gradually decreases due to gravity dominated collapse of smaller, weaker crater walls (Stopar et al., 2017). What we are truly interested in is depth of excavation ( $d_e$ ) (Fig. 4a) as opposed to apparent depth of the crater ( $d$ ) (Fig. 4b). Melosh (1989) indicates that depth of excavation of simple craters with a diameter  $< 15$  km is 10% of the diameter of the transient crater ( $D_t$ ), which is 84% of the apparent diameter of the crater ( $D$ ) yielding the following:

$$d_e \approx 0.1 D_t \quad [38] \tag{2}$$

$$D_t = 0.84 D \quad [38] \tag{3}$$

$$\Rightarrow d_e \approx (0.84) (0.1) D = 0.084 D \tag{4}$$

Using these estimates, we get a depth of excavation equal to 8.4% of the apparent diameter of a small, simple crater.

### 3. Results

Our dataset has a much lower density of cold spot craters for diameters  $> 500$  m than diameters  $< 500$  m (Figs. 3 and 5, Fig. 6). Fig. 5b also shows a significant overlap in the mare and highlands NRA values across crater diameter. To see trends within smaller diameter ranges, and separate out diameters  $> 500$  m where there is less data ( $n = 45$ ), we

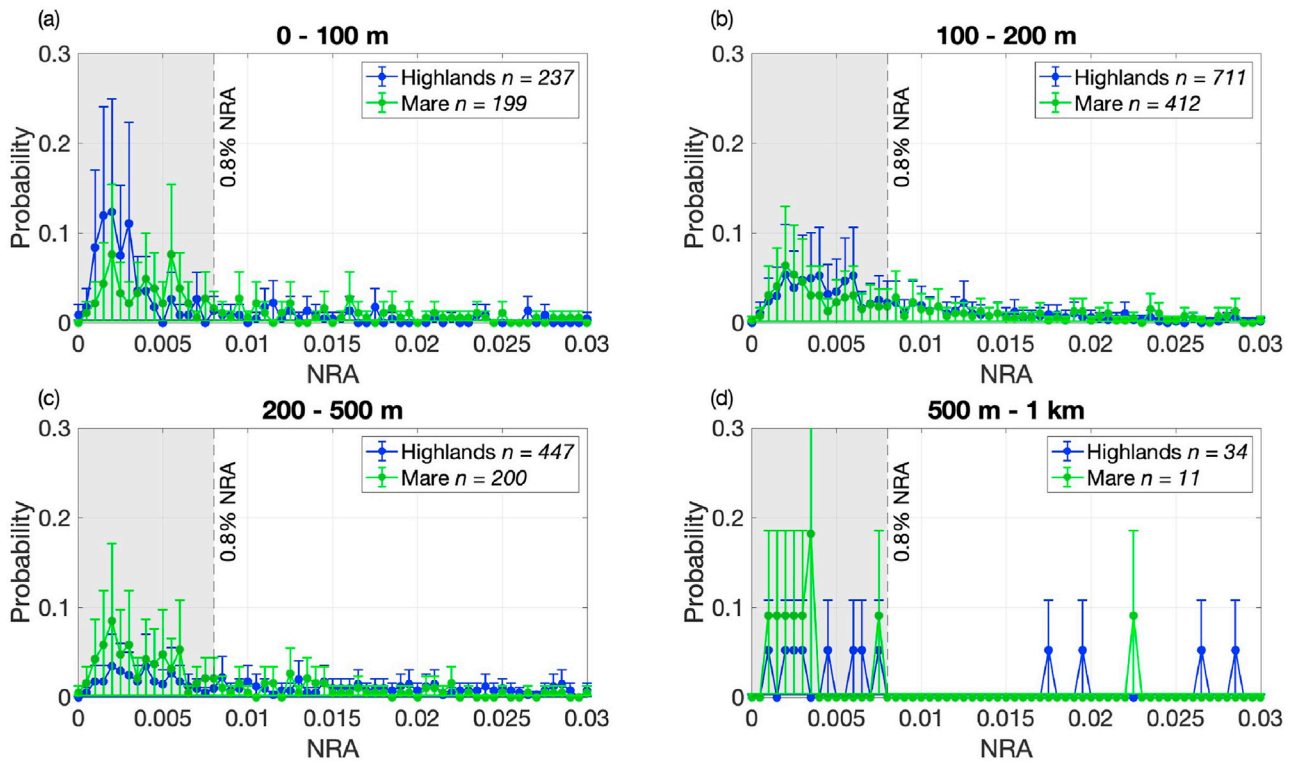


**Fig. 6.** NRA distributions by diameter for the mare and highlands: (a) 0–100 m, (b) 100–200 m, (c) 200–500 m, and (d) 500 m–1 km. Plots have a bin width of 0.05% NRA, with error bars representing the 95% confidence interval. The dashed black line represents our selected threshold for rockiness fraction, which we define as the probability that a given crater has an NRA value greater than 0.8%. Our NRA values extend out to 8% but we have only included values up to 3% for the sake of clarity.

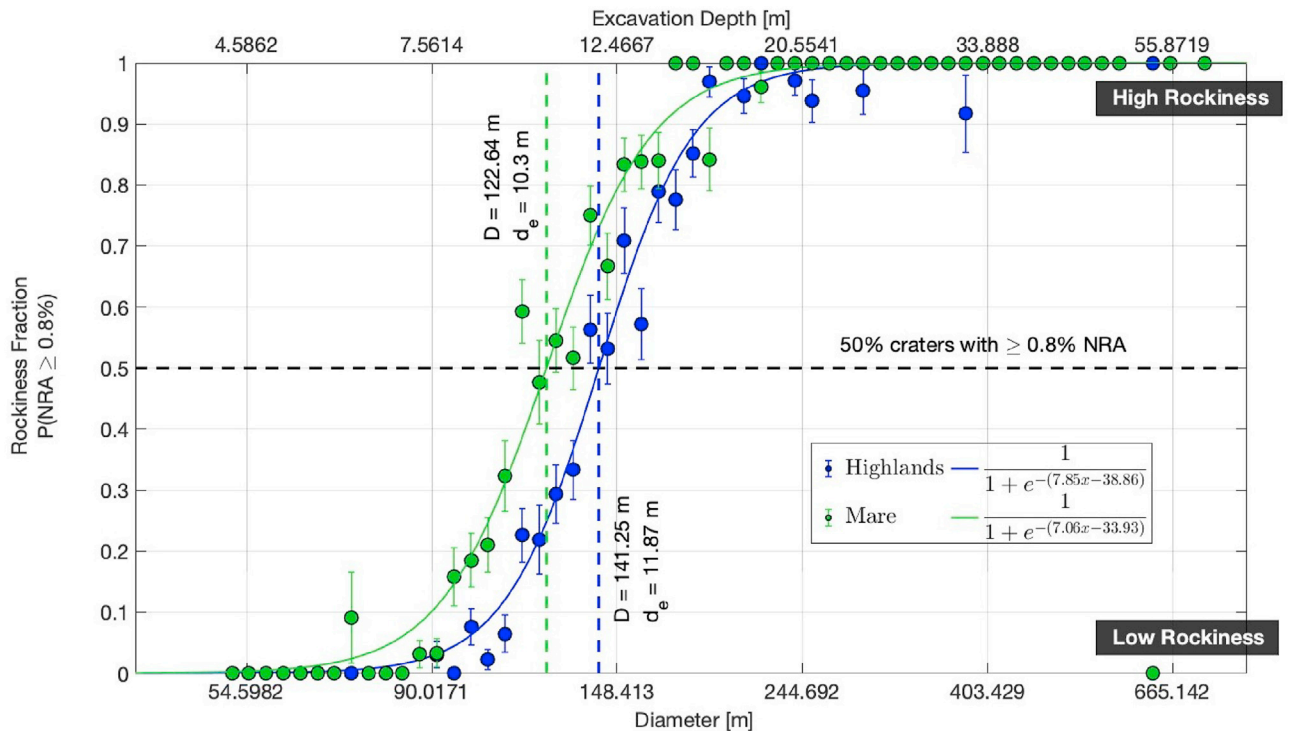


**Fig. 7.** Rockiness fraction by crater diameter (semi-logged along diameter, with log-space diameter binning) and excavation depth for the lunar mare and highlands. Each green and blue marker represents  $P(NRA \geq 0.8\%)$  for each diameter bin in the mare and highlands respectively. The green and blue solid curves are Sigmoid fits for those regions. The error bars represent the 95% confidence interval of the rockiness fraction.

compare NRA distributions by diameter (Fig. 6). This also allows us to see potential differences between the mare and highlands regions.

### 3.1. Threshold selection and rockiness fraction

From Fig. 6a, b, and c, we see that for the smallest diameters, majority craters have NRA  $\leq 0.8\%$ . Our approach for identifying rocky craters requires choosing a 'rockiness' decision threshold, below which craters are considered not rocky and above which they are considered rocky. A threshold of 0.8% NRA is therefore selected, and we define the probability that a given crater has an NRA value greater than 0.8% as the rockiness fraction:

$$P(NRA \geq 0.8\%) \quad (5)$$

In other words, a low rockiness fraction or probability indicates a low NRA for that particular diameter range, while a high rockiness fraction or probability represents a high NRA for the same. This threshold can be refined in future studies with the availability of more data (Behrens et al., 2004; Sohn et al., 2005).

### 3.2. Mare and highlands depths

Plotting the rockiness fraction against crater diameter and excavation depth gives us slightly more discernible differences between the mare and the highlands (Fig. 7). The rockiness fractions for both the mare and highlands fit well with a Logistic Sigmoid function, typically used in statistics and machine learning to model how the probability of an event (a binary, dependent variable) might be affected by one or more explanatory variables (Cramer, 2004). If half the craters in a particular diameter bin are rocky (rockiness fraction = 0.5), we consider this to be an indication of rock excavation detectable by Diviner. The results show that 50% of craters are rocky at a diameter of around 123 m in the mare, and 141 m in the highlands. In accordance with Melosh (1989), these correspond to excavation depths of around 10 and 12 m respectively. Lunar mare craters seem, on average, to become rocky at slightly shallower depths than those on the highlands. It is important to note that these depths are calculated from existing models as opposed to from imaging or other instrument data.

## 4. Discussion

From our results, we see that there is evidence of a slight difference between the mare and highlands excavation depth estimates. However, we still do not completely understand the geology of the regolith-bedrock interface in either region. For instance, there is still debate as to whether a megaregolith or paleoregolith might exist, and if it's interspersed with finer regolith or completely buried beneath it. The presence of a megaregolith or shock-lithified breccia boulders could pose a challenge to regolith thickness estimates from Diviner. Detected rock could potentially include highly friable breccia thought to have been formed from regolith crystallization upon impact (Muehlberger et al., 1973; Schmitt, 1973). However, we expect friable breccia to have a lower thermal inertia than coherent rock (Elder et al., 2019), and therefore not significantly affect our results. The presence of impact melt deposits in small, simple impact craters in the lunar highlands that either partly or completely bury rocks (Plescia and Cintala, 2012), could also impact regolith thickness estimates from Diviner. Even so, these melt deposits are rare, and unlikely to significantly affect our results. It is also useful to note that with recent growing interest in lunar pits (Horvath et al., 2022), further analysis and in-situ work on these mare cave openings could help constrain the regolith thickness in those regions.

Our excavation depth estimates are unique values for both the mare and highlands regions. It is worth noting that interpreting these results in terms of a single regolith thickness can be problematic. Firstly, regolith

thickness estimates are not only varied across techniques, but also spatially within a local area on the lunar surface (Wilcox et al., 2005; Wilhelms and with, 1987). Secondly, we must rely on existing excavation depth models (Melosh, 1989) to estimate these thicknesses. Sharpton (2014) has suggested a new model based on higher resolution LROC images showing crater deformation that suggest a depth of excavation less than or equal to 3% of the diameter of the transient crater.

$$d_e \leq 0.03 D_r [49] \quad (6)$$

$$\Rightarrow d_e \approx (0.84) (0.03) D = 0.025 D \quad (7)$$

Using Sharpton's results would give a depth of excavation of 2.52% of the apparent diameter of a small, simple crater. Melosh's model (Melosh, 1989) gives us regolith thickness estimates that are more than three times those of Sharpton's. However, both models give us estimates that are within the range of other previous studies (Fa and Wieczorek, 2012; Hörz et al., 1991; Shkuratov and Bondarenko, 2001; Quaide and Oberbeck, 1968; Bart et al., 2011; Wilcox et al., 2005; Shoemaker and Morris, 1970).

## 5. Conclusion

Our results show that the mare regolith might be thinner than that in the highlands. The approximate diameter at which the majority of craters start to become rocky is 123 m in the mare and 141 m in the highlands. Using maximum excavation depth estimations from Melosh (1989), this corresponds to a 10 m average rock-free regolith thickness in the mare and 12 m in the highlands. Using maximum excavation depth estimations from Sharpton (2014), we get 3 m average rock-free regolith thickness in the mare, and 4 m in the highlands. Both models give us regolith thickness estimates that are within the range of other previous estimates (Fa and Wieczorek, 2012; Hörz et al., 1991; Shkuratov and Bondarenko, 2001; Quaide and Oberbeck, 1968; Bart et al., 2011; Wilcox et al., 2005; Shoemaker and Morris, 1970) which is significant in that our approach to estimating regolith thickness differs from previous ones, while producing results consistent with them.

### Author statement/agreement

All authors have seen and approved the final version of the manuscript being submitted. They warrant that the article is the authors' original work, hasn't received prior publication, and isn't under consideration for publication elsewhere.

### Declaration of competing interest

The authors declare that they have no known competing financial interests or personal relationships that could have appeared to influence the work reported in this paper.

### Data availability

Our data 'Diviner Normalized Rock Abundance Data' is publicly available on Mendeley (Venkatraman et al., 2022). Our code is also publicly available on GitHub (Venkatraman, 2022). The LROC and other Diviner data products used are publicly available via the LROC Data Node (<https://wms.lroc.asu.edu/lroc/rdr/product/select>) and the Geosciences Node of the Planetary Data System ([https://pds-geosciences.wustl.edu/286\\_missions/lro/diviner.htm](https://pds-geosciences.wustl.edu/286_missions/lro/diviner.htm)).

### Acknowledgments

We thank Catherine Elder and Ben Douglass for their complementary contributions and insight regarding Diviner regolith thickness estimates.

We also thank the LROC team, Jean-Pierre Williams, and Joshua L. Bandfield for their data. We benefited from helpful comments and feedback from the Diviner team, and edits by Jacob Widmer.

## Appendix A. Supplementary data

Supplementary data to this article can be found online at <https://doi.org/10.1016/j.pss.2023.105662>.

## References

- Apollo 11 mission report, 1969. Tech. Rep. National Aeronautics and Space Administration, Manned Spacecraft Center, Houston, TX, USA.
- Apollo 12 mission report, 1970. Tech. Rep. National Aeronautics and Space Administration, Manned Spacecraft Center, Houston, TX, USA.
- Arnold, J.R., 1975. A Monte Carlo model for the gardening of the lunar regolith. *Moon* 13, 159–172. <https://doi.org/10.1007/BF00567513>.
- Bandfield, J.L., Ghent, R.R., Vasavada, A.R., Paige, D.A., Lawrence, S.J., Robinson, M.S., 2011. Lunar surface rock abundance and regolith fines temperatures derived from Iro diviner radiometer data. *J. Geophys. Res.: Planets* 116 (E12). <https://doi.org/10.1029/2011JE003866>.
- Bandfield, J.L., Song, E., Hayne, P.O., Brand, B.D., Ghent, R.R., Vasavada, A.R., Paige, D.A., 2014. Lunar cold spots: granular flow features and extensive insulating materials surrounding young craters. *Icarus* 231, 221–231. <https://doi.org/10.1016/j.icarus.2013.12.017>.
- Bart, G.D., Nickerson, R.D., Lawder, M.T., Melosh, H., 2011. Global survey of lunar regolith depths from Iroc images. *Icarus* 215 (2), 485–490. <https://doi.org/10.1016/j.icarus.2011.07.017>.
- Basilevsky, A., Head, J., Horz, F., 2013. Survival times of meter-sized boulders on the surface of the moon. *Planet. Space Sci.* 89, 118–126. <https://doi.org/10.1016/j.pss.2013.07.011>.
- Behrens, C.N., Hedibert, F.L., Gamerman, D., 2004. Bayesian analysis of extreme events with threshold estimation. *Stat. Model. Int. J.* 4 (3), 227–244. <https://doi.org/10.1191/1471082X04st0750a>.
- Cintala, M.J., McBride, K.M., 1995. Block Distributions on the Lunar Surface: A Comparison between Measurements Obtained from Surface and Orbital Photography. Tech. Rep. 104804. NASA Johnson Space Center, Houston, TX.
- Colaprete, A., Schultz, P., Heldmann, J., Wooden, D., Shirley, M., Ennico, K., Hermaly, B., Marshall, W., Ricco, A., Elphic, R.C., Goldstein, D., Summy, D., Bart, G.D., Asphaug, E., Korycansky, D., Landis, D., Sollitt, L., 2010. Aricebo radar mapping of the lunar poles: a search for ice deposits. *Science* 330 (6003), 463–468. <https://doi.org/10.1126/science.1186986>.
- Cramer, J.S., 2004. The early origins of the logit model. *Stud. Hist. Philos. Biol. Biomed. Sci.* 35, 613–626. <https://doi.org/10.1016/j.shpsc.2004.09.003>.
- Elder, C.M., Douglass, B., Ghent, R.R., Hayne, P.O., Williams, J.-P., Bandfield, J.L., Costello, E., 2019. The subsurface coherent rock content of the moon as revealed by cold-spot craters. *J. Geophys. Res.: Planets* 124, 3373–3384. <https://doi.org/10.1029/2019JE006128>.
- Fa, W., Wieczorek, M.A., 2012. Regolith thickness over the lunar nearside: results from earth-based 70-cm aricebo radar observations. *Icarus* 218 (2), 771–787. <https://doi.org/10.1016/j.icarus.2012.01.010>.
- Fa, W., Zhu, M.-H., Liu, T., Plescia, J.B., 2015. Regolith stratigraphy at the chang'e-3 landing site as seen by lunar penetrating radar. *Geophys. Res. Lett.* 42 (23), 10179–10187. <https://doi.org/10.1002/2015GL066537>.
- Fisher, E.A., Lucey, P.G., Lemelin, M., Greenhagen, B.T., Siegler, M.A., Mazarico, E., Aharonson, O., Williams, J.-P., Hayne, P.O., Neumann, G.A., Paige, D.A., Smith, D.E., Zuber, M.T., 2017. Evidence for surface water ice in the lunar polar regions using reflectance measurements from the lunar orbiter laser altimeter and temperature measurements from the diviner lunar radiometer experiment. *Icarus* 292, 74–85. <https://doi.org/10.1016/j.icarus.2017.03.023>.
- Ghent, R.R., Hayne, P.O., Bandfield, J.L., Campbell, B.A., Allen, C.C., Carter, L.M., Paige, D.A., 2014. Constraints on the recent rate of lunar ejecta breakdown and implications for crater ages. *Geology* 42 (12), 1059–1062. <https://doi.org/10.1130/G35926.1>.
- Grieve, R.A.F., 1987. Terrestrial impact structures. *Annu. Rev. Earth Planet Sci.* 15 (1), 245–270. <https://doi.org/10.1146/annurev.ea.15.050187.001333>.
- Hayne, P.O., Hendrix, A., Sefton-Nash, E., Siegler, M.A., Lucey, P.G., Retherford, K.D., Williams, J.-P., Greenhagen, B.T., Paige, D.A., 2015. Evidence for exposed water ice in the moon's south polar regions from lunar reconnaissance orbiter ultraviolet albedo and temperature measurements. *Icarus* 225, 58–69. <https://doi.org/10.1016/j.icarus.2015.03.032>.
- Hayne, P.O., Bandfield, J.L., Siegler, M.A., Vasavada, A.R., Ghent, R.R., Williams, J.-P., Greenhagen, B.T., Aharonson, O., Elder, C.M., Lucey, P.G., Paige, D.A., 2017. Global regolith thermophysical properties of the moon from the diviner lunar radiometer experiment. *J. Geophys. Res.: Planets* 122 (12), 2371–2400. <https://doi.org/10.1002/2017JE005387>.
- Horvath, T., Hayne, P.O., Paige, D.A., 2022. Thermal and illumination environments of lunar pits and caves: models and observations from the diviner lunar radiometer experiment. *Geophys. Res. Lett.* 49 (14). <https://doi.org/10.1029/2022GL099710>.
- Hörz, F., Grieve, R., Heiken, G., Spudis, P., Binder, A., 1991. Lunar Sourcebook - A User's Guide to the Moon. Cambridge University Press, pp. 61–111. Ch. 4.
- Humm, D.C., Tschimmel, M., Brylow, S.M., Mahanti, P., Tran, T.N., Braden, S.E., Wiseman, S., Danton, J., Eliason, E.M., Robinson, M.S., 2016. Flight calibration of the Iroc narrow angle camera. *Space Sci. Rev. Online* 200, 431–473. <https://doi.org/10.1007/s11214-015-0201-8>.
- Li, S., P. G. L., Milliken, R.E., Hayne, P.O., Fisher, E., Williams, J.-P., Hurley, D.M., Elphic, R.C., 2018. Direct evidence of surface exposed water ice in the lunar polar regions. *Proc. Natl. Acad. Sci. USA* 115 (36), 8907–8912. <https://doi.org/10.1073/pnas.1802345115>.
- Mahanti, P., Humm, D.C., Robinson, M.S., Boyd, A.K., Stelling, R., Sato, H., Denevi, B.W., Braden, S.E., Bowman-Cisneros, E., Brylow, S.M., Tschimmel, M., 2016. Inflight calibration of the lunar reconnaissance orbiter camera wide angle camera. *Space Sci. Rev. Online* 200, 393–430. <https://doi.org/10.1007/s11214-015-0197-0>.
- McKay, D.S., Heiken, G., Basu, A., Blanford, G., Simon, S., Reedy, R., French, B.M., Papike, J., 1991. Lunar Sourcebook - A User's Guide to the Moon. Cambridge University Press, pp. 285–356. Ch. 7.
- Melosh, H.J., 1989. Planetary Surface Processes. Oxford University Press, New York, NY, pp. 222–272. Ch. 6.
- Muehlberger, W.R., Batson, R.M., Cernan, E.A., Freeman, V.L., Hait, M.H., Holt, H.E., Howard, K.A., Jackson, E.D., Larson, K.B., Reed, V.S., Rennison, J.J., Schmitt, H.H., Scott, D.H., Sutton, R.L., Stuart-Alexander, D., Swann, G.A., Trask, N.J., Ulrich, G.E., Wilshire, H.G., Wolfe, E.W., 1973. Apollo 17 Preliminary Science Report, 330. NASA Special Paper, pp. 6–71.
- National Aeronautics and Space Administration, 1994. Catalog of Apollo Experiment Operations. Houston, TX.
- National Aeronautics and Space Administration, 2020. Artemis III Science Definition Team Report.
- Oberbeck, V., Quaide, W., Mahan, M., Paulson, J., 1973. Monte Carlo calculations of lunar regolith thickness distributions. *Icarus* 19 (1), 87–107. [https://doi.org/10.1016/0019-1035\(73\)90141-3](https://doi.org/10.1016/0019-1035(73)90141-3).
- Paige, D.A., Foote, M.C., Greenhagen, B.T., Schofield, J.T., Calcutt, S., Vasavada, A.R., Preston, D.J., Taylor, F.W., Allen, C.C., Snook, K.J., Jakosky, B.M., Murray, B.C., Soderblom, L.A., Jau, B., Loring, S., Bulharowski, J., Bowles, N.E., Thomas, I.R., Sullivan, M.T., Avis, C., Jong, E.M.D., Hartford, W., McCleese, D.J., 2010. The lunar reconnaissance orbiter diviner lunar radiometer experiment. *Space Sci. Rev.* 150, 125–160. <https://doi.org/10.1007/s11214-009-9529-2>.
- Plescia, J.B., Cintala, M.J., 2012. Impact melt in small lunar highland craters. *J. Geophys. Res.: Planets* 117 (E12). <https://doi.org/10.1029/2011JE003941>.
- Powell, T.M., Horvath, T., Robles, V.T., Williams, J.-P., Hayne, P.O., Gallinger, C.L., Greenhagen, B.T., McDougall, D.S., Paige, D.A., 2022. Improved Nighttime Temperature and Rock Abundance Maps of the Moon from the Iro Diviner Lunar Radiometer Experiment with a Model for Topographic Removal. Submitted to JGR: Planets.
- Priour, N.C., Rolf, T., Wünnemann, K., Werner, S.C., 2018. Formation of simple impact craters in layered targets: implications for lunar crater morphology and regolith thickness. *J. Geophys. Res.: Planets* 123 (6), 1555–1578. <https://doi.org/10.1029/2017JE005463>.
- Quaide, W.L., Oberbeck, V.R., 1968. Thickness determinations of the lunar surface layer from lunar impact craters. *J. Geophys. Res.* 73 (16), 5247–5270. <https://doi.org/10.1029/JB073i016p05247>.
- Robinson, M.S., 2010. Lunar Reconnaissance Orbiter Camera Experimental Data Record.
- Robinson, M.S., Brylow, S.M., Tschimmel, M., Humm, D., Lawrence, S.J., Thomas, P.C., Denevi, B.W., Bowman-Cisneros, E., Zerr, J., Ravine, M.A., Caplinger, M.A., Ghaemi, F.T., Schaffner, J.A., Malin, M.C., Mahanti, P., Bartels, A., Anderson, J., Tran, T.N., Eliason, E.M., McEwen, A.S., Turtle, E., Jolliff, B.L., Hiesinger, H., 2010. Lunar reconnaissance orbiter camera (Iroc) instrument overview. *Space Sci. Rev.* 150, 81–124. <https://doi.org/10.1007/s11214-010-9634-2>.
- Rubanenko, L., Venkatraman, J., Paige, D.A., 2019. Thick ice deposits in shallow simple craters on the moon and mercury. *Nat. Geosci.* 12 (8), 597–601. <https://doi.org/10.1038/s41561-019-0405-8>.
- Schmitt, H.H., 1973. Apollo 17 report on the valley of taurus-littrow. *Science* 182 (4113), 681–690. <https://doi.org/10.1126/science.182.4113.681>.
- Sharpton, V.L., 2014. Outcrops on lunar crater rims: implications for rim construction mechanisms, ejecta volumes and excavation depths. *J. Geophys. Res.: Planets* 119 (1), 154–168. <https://doi.org/10.1002/2013JE004523>.
- Shkuratov, Y.G., Bondarenko, N.V., 2001. Regolith layer thickness mapping of the moon by radar and optical data. *Icarus* 149 (2), 329–338. <https://doi.org/10.1006/icar.2000.6545>.
- Shoemaker, E., Morris, E.C., 1970. Physical characteristics of the lunar regolith determined from surveyor television observations. *Radio Sci.* 5 (2), 129–155. <https://doi.org/10.1029/RS005i002p0129>.
- Sohn, H., Allen, D.W., Worden, K., Farrar, C.R., 2005. Structural damage classification using extreme value statistics. *J. Dyn. Syst. Meas. Control* 127, 125–132. <https://doi.org/10.1115/1.1849240>.
- Stopar, J.D., Robinson, M.S., Barnouin, O.S., McEwen, A.S., Speyerer, E.J., Henriksen, M.R., Sutton, S.S., 2017. Relative depths of simple craters and the nature of the lunar regolith. *Icarus* 298, 34–48. <https://doi.org/10.1016/j.icarus.2017.05.022>.
- Venkatraman, J., 2022. Lunar Regolith Thickness. URL. <https://github.com/Jsci96/Lunar-Regolith-Thickness.git>.
- Venkatraman, J., Horvath, T., Powell, T., Paige, D.A., 2022. Diviner Normalized Rock Abundance Data. <https://doi.org/10.17632/b4cyw94t5j.2>.

- Wilcox, B.B., Robinson, M.S., Thomas, P.C., Hawke, B.R., 2005. Constraints on the depth and variability of the lunar regolith. *Meteoritics Planet Sci.* 40 (5), 695–710. <https://doi.org/10.1111/j.1945-5100.2005.tb00974.x>.
- Wilhelms, D.E., with, J.F., 1987. Sections by McCauley, N. J. Trask, the geologic history of the moon. Tech. rep. <https://doi.org/10.3133/pp1348>.
- Williams, J.-P., Paige, D.A., Greenhagen, B.T., Sefton-Nash, E., 2017. The global surface temperatures of the moon as measured by the diviner lunar radiometer experiment. *Icarus* 283. <https://doi.org/10.1016/j.icarus.2016.08.012>.
- Williams, J.-P., Bandfield, J.L., Paige, D.A., Powell, T.M., Greenhagen, B.T., Taylor, S., Hayne, P.O., Speyerer, E.J., Ghent, R.R., Costello, E.S., 2018. Lunar cold spots and crater production on the moon. *J. Geophys. Res.: Planets* 123 (9), 2380–2392. <https://doi.org/10.1029/2018JE005652>.